Relativistic calculations of double K-shell-photoionization cross sections for neutral medium-Z atoms

V. A. Yerokhin,[1,2] A. Surzhykov,[2] and S. Fritzsche[2,3]

[1]*Center for Advanced Studies, St. Petersburg State Polytechnical University, 195251 St. Petersburg, Russia*
[2]*Helmholtz-Institut Jena, D-07743 Jena, Germany*
[3]*Theoretisch-Physikalisches Institut, Friedrich-Schiller-Universität Jena, D-07743 Jena, Germany*

Fully relativistic calculations are presented for the double K-shell photoionization cross section for several neutral medium-Z atoms, from magnesium ($Z = 10$) up to silver ($Z = 47$). The calculations take into account all multipoles of the absorbed photon as well as the retardation of the electron-electron interaction. The approach is based on the partial-wave representation of the Dirac continuum states and uses the Green's-function technique to represent the full Dirac spectrum of intermediate states. The method is strictly gauge invariant, which is used as an independent cross-check of the computational procedure. The calculated ratios of the double-to-single K-shell ionization cross sections are compared with the experimental data and with previous computations.

I. INTRODUCTION

Double photoionization is a fundamental atomic process in which a *single* photon, being absorbed by an atom, simultaneously kicks out *two* electrons. The characteristic feature of this process is that it can proceed only through the electron-electron interaction. Indeed, the incoming photon can (formally) interact only with one electron, so for the second electron to be kicked out, the required energy should be transferred from one electron to another through the electron-electron interaction. This feature makes the double photoionization very sensitive to the details of the electron-electron interaction.

A typical system for studying double photoionization has long been the helium atom, for which numerous experimental and theoretical investigations have been performed [1]. The most widely studied quantity was the ratio of the double-to-single photoionization cross sections σ^{++}/σ^{+} as a function of the energy of the incoming photon ω. Today, the helium double photoionization is often considered as well understood, and the results of several independent computations [2–5] agree reasonably well with the experimental data [6–9] in the whole region of the photon energies.

Unlike the helium case, an adequate description of double photoionization of both K-shell electrons in neutral medium- and high-Z atoms is much more challenging for theory. This is because of the enhanced relativistic effects (that scale as Z^2) as well as the more complex electronic structure of many-electron atoms. The difficulties of the theory in this case were demonstrated by the experiments of Kanter *et al.* on molybdenum [10] and later also on silver [11], which reported large discrepancies with nonrelativistic calculations and claimed "the need for theoretical treatments to properly deal with such systems." More recently, Hoszowska *et al.* [12,13] presented detailed experimental investigations of the double K-shell photoionization for eight medium-Z atoms in the range $12 \leqslant Z \leqslant 23$. In the absence of suitable *ab initio* calculations, the experimental data of Refs. [12] and [13] were interpreted only in terms of various semiempirical models.

An attempt for a systematic *ab initio* calculation of the double K-shell photoionization in neutral atoms was reported by Kheifets *et al.* [14]. In that work, nonrelativistic close-coupling calculations were performed with three gauges of the electromagnetic operator: length, velocity, and acceleration. Convergence (or the lack of it) between the calculations in the different gauges is commonly used as a test of the accuracy of the treatment of the electron correlation. The calculations of Ref. [14] showed that deviations of double-photoionization results obtained in different gauges are large and becoming even larger as the nuclear charge and/or the photon energy are increased. The authors [14] concluded that "significant difficulties" arise and that "none of the available ground-state wave functions satisfied the strict gauge convergence test."

In a previous study of two of us [15], a calculation of the double photoionization was performed within a fully relativistic framework, for which the problem of gauge dependence does not arise as the formalism is gauge invariant from the very beginning. Large relativistic effects were demonstrated in that work, but results were reported only for the He-like ions. In the present investigation, we extend our previous approach to many-electron systems and present fully relativistic calculation of the double K-shell photoionization cross section in neutral atoms.

The computational approach is based on the relativistic QED perturbation theory. It takes into account all multipoles of the absorbed photon as well as the retardation (the frequency dependence) of the electron-electron interaction. The electron-electron interaction is accounted for rigorously to the leading order of perturbation expansion. The higher-order electron-electron interaction (in particular, the interaction with the spectator electrons) is taken into account approximately by means of a suitable screening potential in the Dirac equation.

The remaining paper is organized as follows. In Sec. II we briefly describe our theoretical approach. Section III presents details of the calculation. Numerical results are presented and discussed in Sec. IV. The relativistic units ($\hbar = c = m = 1$) are used throughout this paper.

II. THEORY

We consider the process in which an incoming photon with energy ω and helicity λ collides with a neutral atom and kicks

out *two* electrons from the K shell into the continuum. The final-state electrons have energies ε_1 and ε_2 and momentum $\boldsymbol{p}_1$ and $\boldsymbol{p}_2$, respectively. Such a process can occur when the photon energy ω is equal to or greater than the threshold energy ω_{cr}, which is the (double) ionization energy of the K shell.

The energy-differential cross section of the double K-shell photoionization is given by [15]

$$\frac{d\sigma^{++}}{d\varepsilon_1} = \frac{4\pi^2\alpha}{\omega} \sum_{\kappa_1\kappa_2\mu_1\mu_2} \left| \tau_\lambda^{++}(\varepsilon_1\kappa_1\mu_1,\varepsilon_2\kappa_2\mu_2;\omega) \right|^2, \quad (1)$$

where τ_λ^{++} is the amplitude of the process. The summation in the above formula runs over the partial waves of the continuum wave functions of the ejected (final-state) electrons, i.e., the relativistic angular quantum numbers $\kappa_{1,2}$ and the projections of the total angular momentum $\mu_{1,2}$. The remaining $N-2$ (spectator) electrons do not change their state during the ionization process.

Since the two outgoing electrons share the excess energy of the photoionization process, the *total cross section* is obtained as the integral of the single-differential cross section over a half of the energy-sharing interval

$$\sigma^{++} = \int_m^{m+(\omega-\omega_{cr})/2} d\varepsilon_1 \, \frac{d\sigma^{++}}{d\varepsilon_1}, \quad (2)$$

where ω_{cr} denotes the threshold of the double-photoionization process. The other half of the energy interval corresponds to interchanging the first and the second electron and is accounted for by the antisymmetrized electron wave function.

To the leading order of QED perturbation theory, the amplitude of the double-photoionization process is represented by the two Feynman diagrams as displayed in Fig. 1. The general expression for the amplitude was derived in Ref. [15] by using the two-time Green's-function method [16]:

$$\tau_\lambda^{++} = N \sum_{\mu_a\mu_b} C_{j_a\mu_a \, j_b\mu_b}^{J_0M_0} \sum_{PQ} (-1)^{P+Q}$$

$$\times \sum_n \left\{ \frac{\langle P\varepsilon_1 \, P\varepsilon_2 | I(\Delta_{P\varepsilon_2 \, Qb})|n \, Qb\rangle \, \langle n|R_\lambda|Qa\rangle}{\varepsilon_{Qa} + \omega - \varepsilon_n(1-i0)} \right.$$

$$\left. + \frac{\langle P\varepsilon_1|R_\lambda|n\rangle \, \langle n \, P\varepsilon_2 | I(\Delta_{P\varepsilon_2 \, Qb})|Qa \, Qb\rangle}{\varepsilon_{P\varepsilon_1} - \omega - \varepsilon_n(1-i0)} \right\}. \quad (3)$$
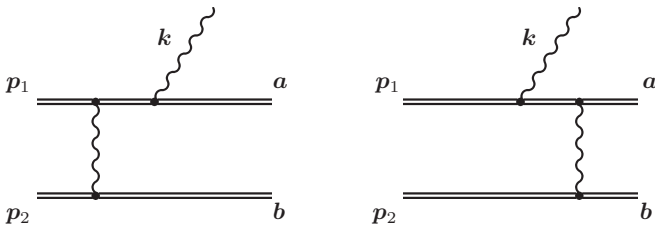

FIG. 1. Feynman diagrams that represent the double-photoionization process in the leading order of perturbation theory. a and b denote the bound electron states, $\boldsymbol{p}_1$ and $\boldsymbol{p}_2$ are the continuum electron states, and $\boldsymbol{k}$ refers to the incoming photon. Double lines denote electrons that are propagating in a central potential (nuclear Coulomb field plus some screening potential). Proper antisymmetrization of the initial and the final two-electron wave functions is assumed.

The operators in the matrix elements in the above formula are the frequency-dependent electron-electron interaction operator $I(\Delta)$ and the operator of the photon absorption R_λ. The states $|a\rangle \equiv |\kappa_a\mu_a\rangle$ and $|b\rangle \equiv |\kappa_b\mu_b\rangle$ describe the initial bound electron states, whereas $|\varepsilon_1\rangle \equiv |\varepsilon_1\kappa_1\mu_1\rangle$ and $|\varepsilon_2\rangle \equiv |\varepsilon_2\kappa_2\mu_2\rangle$ describe the final continuum electron states with a definite total angular momentum.

The first term in the curly brackets of Eq. (3) corresponds to the diagram with the electron-electron interaction attached to the final-state electron wave function (the left graph in Fig. 1) and the second one, to the diagram with the electron-electron interaction attached to the initial-state electron wave function (the right graph in Fig. 1). The summation over P and Q in Eq. (3) corresponds to the permutation of the initial and final electrons; $P\varepsilon_1 P\varepsilon_2 = (\varepsilon_1\varepsilon_2)$ or $(\varepsilon_2\varepsilon_1)$, $QaQb = (ab)$ or (ba), and $(-1)^P$ and $(-1)^Q$ are the permutation signs. The summation over n in Eq. (3) runs over the complete Dirac spectrum of intermediate states [16]; $\Delta_{\varepsilon_i b} \equiv \varepsilon_i - \varepsilon_b$, $N = 1/\sqrt{2}$ for the equivalent initial-state electrons and $N = 1$ otherwise; $j_{a,b}$ and $\mu_{a,b}$ are the total angular momentum and its projection of the initial-state electrons; and J_0 and M_0 are the total angular momentum of the initial two-electron state and its projection. In the case of the K shell, $N = 1/\sqrt{2}$, $J_0 = M_0 = 0$, $j_a = j_b = 1/2$.

The general relativistic expression for the photon absorption operator R_λ is given by

$$R_\lambda = \boldsymbol{\alpha} \cdot \hat{\boldsymbol{u}}_\lambda \, e^{i\boldsymbol{k}\cdot\boldsymbol{r}} + G(\boldsymbol{\alpha} \cdot \hat{\boldsymbol{k}} - 1) \, e^{i\boldsymbol{k}\cdot\boldsymbol{r}}, \quad (4)$$

where $\boldsymbol{\alpha}$ is a three-component vector of the Dirac matrices, $\hat{\boldsymbol{u}}_\lambda$ is the polarization vector of the absorbed photon, $\boldsymbol{k}$ is the photon momentum, $\hat{\boldsymbol{k}} = \boldsymbol{k}/|\boldsymbol{k}|$, and G is the gauge parameter.

The relativistic frequency-dependent electron-electron interaction operator in the Feynman gauge is given by

$$I^{\text{Feyn}}(\omega) = \alpha(1 - \boldsymbol{\alpha}_1 \cdot \boldsymbol{\alpha}_2) \frac{e^{i|\omega|x_{12}}}{x_{12}}, \quad (5)$$

where $x_{12} = |\boldsymbol{x}_1 - \boldsymbol{x}_2|$. In the Coulomb gauge, the electron-electron interaction acquires an additional term:

$$I^{\text{Coul}}(\omega) = I^{\text{Feyn}}(\omega)$$

$$+ \alpha\left[1 - \frac{(\boldsymbol{\alpha}_1 \cdot \boldsymbol{\nabla}_1)(\boldsymbol{\alpha}_2 \cdot \boldsymbol{\nabla}_2)}{\omega^2}\right]\frac{1 - e^{i|\omega|x_{12}}}{x_{12}}. \quad (6)$$

In our approach, all one-electron states in Eq. (3), $|\varepsilon_{1,2}\rangle$, $|a\rangle$, $|b\rangle$, and $|n\rangle$, are assumed to be eigenstates of the same one-particle Dirac Hamiltonian,

$$h_D = \boldsymbol{\alpha} \cdot \boldsymbol{p} + (\beta - 1)m + V_{\text{nuc}}(r) + V_{\text{scr}}(r), \quad (7)$$

where β is the Dirac β matrix, $\boldsymbol{p}$ is the momentum operator, V_{nuc} is the binding potential of the nucleus, and V_{scr} is the screening potential induced by the presence of other electrons. So our approach includes the electron-electron interaction to the first order of the QED perturbation theory exactly, whereas the higher-order electron-electron interactions are accounted for approximately, through the screening potential in the Dirac equation. By varying the definition of the screening potential, we can estimate the residual electron correlation effects that are omitted in the present treatment.

In the present work, we construct the screening potential by first solving the Dirac-Fock equation for the neutral atom and

then generating the potential as it arises from the charge density of the Dirac-Fock orbitals weighted by the occupation numbers of the orbitals. In particular, we make use of two variants of the potential which will be termed as the core-Hartree (CH) potentials $V_{\mathrm{CH},1}(r)$ and $V_{\mathrm{CH},2}(r)$ and which are defined by

$$
\begin{aligned}
V_{\mathrm{CH},K}(r) = \alpha \int_0^\infty dr' \frac{1}{\max(r,r')} \\
\times \sum_n (q_n - K \, \delta_{na}) \left[G_n^2(r) + F_n^2(r) \right], \quad (8)
\end{aligned}
$$

where $K = 1$ or 2, n numerates the one-electron orbitals, q_n is the occupation number of the orbital, a is the initial $1s$ electron state, and G_n and F_n are the upper and the lower radial components of the Dirac-Fock orbitals.

As can be seen from the definition (8), $V_{\mathrm{CH},2}(r)$ represents the potential generated solely by the charge density of the spectator electrons that do not change their state during the process, whereas $V_{\mathrm{CH},1}(r)$ includes in addition the interaction with the second $1s$ electron in the K shell.

It is important that all initial and intermediate states in our approach are the exact eigenstates of the same one-particle Dirac Hamiltonian h_D with the potential $V_{\mathrm{nuc}}(r) + V_{\mathrm{scr}}(r)$. Because of this and the fact that the screening potential V_{scr} constructed by Eq. (8) is a *local* potential, the amplitude (3) is *gauge invariant*. We note that if we had used a nonlocal (e.g., Dirac-Fock) screening potential in h_D, it would have broken the gauge invariance [17].

It can be proved that the amplitude (3) is separately gauge invariant with respect to the gauge of the absorbed photon as well as the gauge of the electron-electron interaction. This gauge invariance was used in order to check our numerical procedure. In addition, the gauge invariance provides us with a cross-check of the computation of the two Feynman diagrams against each other. Indeed, while the contributions of the two diagrams in Fig. 1 are different for different gauges of the emitted photon, their sum should be (and was checked numerically to be) the same.

III. NUMERICAL ISSUES

A general (numerical) scheme for the computation of double-photoionization cross sections was developed in our previous investigation [15]. Similarly to that, the summation over the complete spectrum of the Dirac equation is performed in the present work by using the Dirac-Green's function. The distinct feature of the present computation is that the initial and final states as well as the Dirac-Green's function need to be calculated not only for the point-nucleus Coulomb potential (as in Ref. [15]), but for some general (Coulomb+screening) potential. For the wave functions, such a generalization is quite straightforward, and these functions can be readily obtained, e.g., with the help of the FORTRAN package developed by Salvat *et al.* [18]. In contrast, an efficient computation of the Dirac-Green's function for the general potential is more difficult.

For a given value of the relativistic angular quantum number κ, the radial part of the Dirac-Green's function is represented in terms of the two-component solutions of the radial Dirac

equation that are regular at the origin (ϕ_κ^0) and at infinity (ϕ_κ^∞):

$$
\begin{aligned}
G_\kappa(E,r_1,r_2) = &-\phi_\kappa^\infty(E,r_1) \, \phi_\kappa^{0T}(E,r_2) \, \theta(r_1 - r_2) \\
&-\phi_\kappa^0(E,r_1) \, \phi_\kappa^{\infty T}(E,r_2) \, \theta(r_2 - r_1), \quad (9)
\end{aligned}
$$

where E denotes the energy argument of the Green's function, r_1 and r_2 are the radial arguments, and θ is the Heaviside step function.

An efficient numerical scheme for computing the regular and irregular solutions of the Dirac equation for an arbitrary Coulomb + short-range potential was developed by one of us in Ref. [19]. We note that practical computations for arbitrary potential become much more time consuming as compared to computations with the point-nucleus Coulomb potential. The reason is that the point-nucleus Dirac-Coulomb-Green's function can be calculated directly at any radial point, whereas for arbitrary potential, a two-step procedure is required: first one needs to solve the radial Dirac equation on the grid and only then one can obtain the regular and irregular Dirac solutions by interpolation.

A serious numerical problem arises in the evaluation of the radial integrals for the left graph in Fig. 1 (where the electron correlation modifies the final-state wave function). In this case, the continuum-state Dirac wave function has to be integrated together with the Dirac-Green's function with the energy $E > m$. All functions under the integral are strongly oscillating and decrease only (very) slowly for large radial arguments. It is therefore practically impossible to evaluate such integrals to high precision by just applying a straightforward numerical integration. In our approach, we use instead the method of the complex-plane rotation of the integration contour, described in detail in Ref. [20].

After the radial integrals are successfully evaluated, the next problem is the summation of the partial-wave expansions. When all angular momentum selection rules are taken into account, two (out of five) partial-wave summations remain infinite. One can choose the parameters for these two infinite summations differently. Our choice was the relativistic angular momentum parameters κ_1 and κ_2 of the two final-state electrons in Eq. (1). In the present work, the number of partial waves included was $(|\kappa_1|, |\kappa_2|) = (10, 10)$, with the tail of the expansion estimated by extrapolation. This is slightly less than in our previous investigation [15], since the maximal photon energy is smaller in the present work.

A number of tests have been performed in order to check our numerical procedure. First, we checked the gauge invariance of the calculated results. Apart from the Feynman gauge which was normally used, we repeated our calculations with the electron-electron interaction in the Coulomb gauge [see Eq. (6)] and found perfect agreement. We also checked that varying the gauge of the absorbed photon [parameter G in Eq. (4)] has no effect on the numerical results. Second, we recalculated the contribution of the right diagram in Fig. 1 by using a completely different numerical technique, based on the explicit summation over the Dirac spectrum represented by the finite basis set of B splines [21]. Finally, we checked the nonrelativistic limit of our calculations for the point-nucleus Coulomb potential against the independent perturbation-theory calculations of Mikhailov *et al.* [22] and Amusia *et al.* [23] and found good agreement.

TABLE I. K-shell double-ionization energy ω_{cr}, in keV.

Z	CH_1	CH_2	Coul	MCDF	Ref. [25]
12	2.65	3.05	3.93	2.79	2.61
20	8.12	8.79	10.9	8.39	8.09
29	18.0	19.0	23.2	18.4	18.0
47	51.1	52.8	62.0	51.9	51.3

IV. RESULTS AND DISCUSSION

In the present work, we study the process of the double K-shell photoionization for several neutral medium-Z atoms: magnesium ($Z = 12$), calcium ($Z = 20$), copper ($Z = 29$), and silver ($Z = 47$). The results of the calculation are presented in terms of the ratio of the double-to-single K-shell ionization cross section,

$$\mathcal{R} = Z^2 \frac{\sigma^{++}}{\sigma^+} , \qquad (10)$$

as a function of the ratio of the incoming photon energy and the double K-shell photoionization energy $\omega/\omega_{\mathrm{cr}}$. The prefactor of Z^2 in the definition (10) ensures that the function $\mathcal{R}(\omega/\omega_{\mathrm{cr}})$ depends only weakly on the nuclear charge and the degree of ionization of the atom (ion); this fact is often termed as the universal scaling law of double photoionization [26,27]. In our previous calculation for He-like ions [15], we demonstrated that this scaling holds exactly in the *nonrelativistic limit* and to the *first order* in perturbation theory, but is violated by the relativistic effects.

In order to obtain numerical results for $\mathcal{R}(\omega/\omega_{\mathrm{cr}})$, we need first to calculate the double K-shell ionization energy ω_{cr} and the cross section of the usual (single) K-shell photoionization σ^+. These calculations are relatively simple and can be performed by many different methods. In the present investigation, however, we required that ω_{cr} and σ^+ be calculated within exactly the same approach as the double-photoionization cross section σ^{++}.

In Tables I and II, we present numerical results for the K-shell double-ionization energy ω_{cr} and the cross section of the single K-shell photoionization σ^+ for $\omega = 2\omega_{\mathrm{cr}}$, respectively. The columns labeled CH_1, CH_2, and Coul display the data obtained in the present work with the corresponding potential in the Dirac equation ($V_{\mathrm{CH},1}$, $V_{\mathrm{CH},2}$, and the Coulomb potential, respectively). The Coulomb-potential values correspond to the case of He-like ion in the independent particle model. The data in the MCDF column are obtained by the multiconfigurational Dirac-Fock method by using the RATIP package [24], whereas the data in the last column are taken from the literature [25].

TABLE II. Cross section of single K-shell photoionization σ^+ for the photon energy $\omega = 2\omega_{\mathrm{cr}}$, in kbarn.

Z	CH_1	CH_2	Coul	MCDF	Ref. [25]
12	4.88	3.55	1.70	4.95	5.40
20	1.38	1.15	0.61	1.40	1.52
29	0.575	0.510	0.288	0.635	0.649
47	0.183	0.171	0.108	0.188	0.189

TABLE III. Ratio of the double-to-single K-shell-photoionization cross sections $\mathcal{R} = Z^2 \sigma^{++}/\sigma^+$, for the photon energy $\omega = 2\omega_{\mathrm{cr}}$.

Z	CH_1	CH_2	Coul	Coul (NR)
12	0.340	0.286	0.200	0.191
20	0.316	0.287	0.214	0.191
29	0.323	0.305	0.239	0.191
47	0.383	0.373	0.318	0.191

The single-photoionization cross sections CH_1, CH_2, and Coul are obtained within the single-electron approximation, where the electron-electron interaction is accounted for approximately either through the screening potential (for the CH_1 and CH_2 values) or is totally ignored (for the Coulomb case). It is thus natural that these results are less accurate than the ones obtained by the MCDF method. As might have been anticipated, the CH_1 potential is the best choice among the three potentials considered. It is important that the difference between the CH_1 and CH_2 values yields a reliable estimate of the residual electron correlation effects neglected by the effective single-electron approximation.

Let us now turn to the main objective of the present work: the ratio of the double-to-single K-shell photoionization cross sections $\mathcal{R}$. Our numerical results for $\mathcal{R}$ are presented in Table III for the photon energy $\omega = 2\omega_{\mathrm{cr}}$ and for the three different potentials, CH_1, CH_2, and Coul. In the last column, we list also the nonrelativistic limit of the Coulomb results. The striking feature of the presented comparison is that the ratio $\mathcal{R}$ is much less sensitive to the choice of the potential than the single-photoionization cross section σ^+. This explains why we took great care in order to calculate σ^{++} and σ^+ fully consistently, i.e., both to the leading order in perturbation theory with exactly the same screening potential in the Dirac equation (7). The importance of such consistency was implicitly acknowledged already in previous perturbation-theory calculations [15,22,23], where results were presented solely in terms of $\mathcal{R}$ and not in terms of σ^{++}.

From the comparison in Tables I–III, we see that the difference between the CH_1 and CH_2 results (which we use for estimating the magnitude of the residual electron correlation effects) monotonically decreases with the increase of the nuclear charge. It is consistent with what one might have anticipated: the single-electron approximation usually performs the better, the heavier the atom under consideration.

The nonrelativistic Coulomb values of $\mathcal{R}$ in Table III are exactly the same for all atoms. This demonstrates the universal scaling law of the *nonrelativistic* double photoionization [26,27]. As seen from the table, the nonrelativistic scaling is violated by the relativistic effects, so that the relativistic Coulomb results depend on nuclear charge.

We now discuss our results for selected atoms in more detail. Figure 2 presents our calculation for magnesium. The left panel compares our results with the nonrelativistic calculations in the length, velocity, and acceleration gauge by Kheifets *et al.* [14], as well as the experiments by Hoszowska *et al.* [12,13]. Our results are shown for the CH_1 (red solid line) and CH_2 (orange dashed line) potentials. In addition,
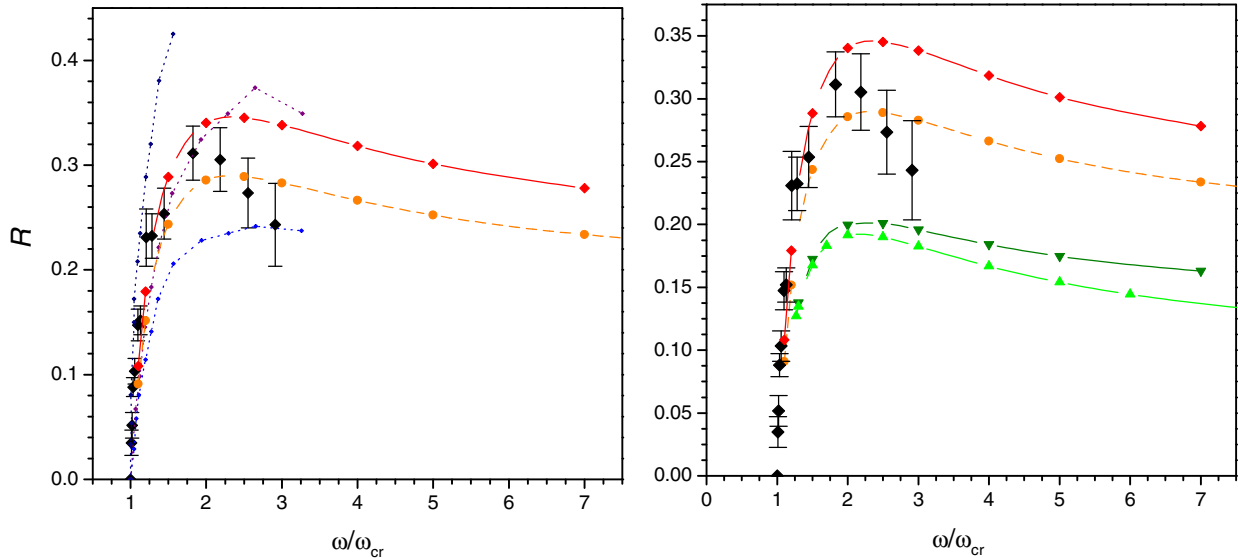
FIG. 2. (Color online) Double K-shell photoionization cross section for neutral magnesium (Mg, $Z = 12$). The double-to-single K-shell ionization ratio ($\mathcal{R} = Z^2\sigma^{++}/\sigma^+$) is plotted as function of the incoming photon energy ω in units of the double K-shell photoionization energy ω_{cr}. The results of the present calculation are plotted by a solid line (red) for the CH_1 potential and by a dashed line (orange) for the CH_2 potential, respectively. The experimental results of Refs. [12] and [13] are shown by black diamond points. On the left panel, the calculations by Kheifets *et al.* [14] in length, velocity, and acceleration gauge are shown by dotted lines (navy, purple, and blue, respectively). On the right panel, the present theory and experiment [12,13] for neutral magnesium are compared with the computations for He-like magnesium ions. The relativistic results for the He-like ion are shown by the down-triangle points (dark green line); the nonrelativistic calculation is shown by the up-triangle points (light green line).

the right panel of this figure displays our calculations for the corresponding He-like ion (Coulomb potential), presenting the relativistic results (dark green, down-triangle points) and nonrelativistic results (light green, up-triangle points). The results for the He-like ions are equivalent to those obtained in our previous work [15].

From the comparison in the right panel of Fig. 2, we can identify the magnitude of various effects. The difference between the nonrelativistic and the relativistic curves for He-like ion shows the effect of relativity, whereas the difference between the CH_2 results for the neutral-atom and the relativistic results for He-like ion identifies the effect of the outer electrons. The difference between the CH_1 and CH_2 curves might be interpreted as the effect of higher-order interactions between the two K-shell electrons. We may therefore conclude that for magnesium, the relativistic effects are not very prominent but the interaction with the outer shells increases the ratio $\mathcal{R}$ by about 50% and thus cannot be neglected.

The results of our calculation for magnesium agree reasonably well with the experimental data [12,13] for energies up to the maximum of the curve ($\omega/\omega_{cr} \approx 2$) but deviate noticeably for higher photon energies. Good agreement is also observed with the nonrelativistic results by Kheifets and co-workers [14], obtained in the velocity gauge, while their results in the acceleration and length gauge deviate significantly, both from our predictions as well as from experimental data.

Figure 3 displays our results for calcium and compares them with previous calculations [14,22] and experiments [12,13,28]. We observe that for this element, neither of the calculations agrees well with experiment. The computations by Kheifets *et al.* [14] exhibit a very strong gauge dependence. At the

same time, similarly as for magnesium, their results in the velocity gauge are found to be in good agreement with our values. The computations by Mikhailov *et al.* [22] agree with our results and with Kheifets's velocity-gauge data for small photon energies of $\omega/\omega_{cr} \lesssim 1.5$ but predict significantly smaller values of $\mathcal{R}$ at higher photon energies.

Figure 4 presents the ratio $\mathcal{R}$ for copper. Results of our relativistic calculation for the neutral atom with the screening potentials CH_1 and CH_2 (the red solid line and the orange dashed line, respectively) are compared with our relativistic calculation for the He-like ion (dark green line, down-triangle points) and the corresponding nonrelativistic calculation (light green line, upper-triangle points). Here our results agree well with the only available experimental point [29] in the near-to-threshold region.

Finally, Fig. 5 presents theoretical and experimental results for silver, which is the heaviest atom for which measurements of the double K-shell photoionization have been performed. We observe that two of the three experimental points reported in Ref. [11] disagree strongly with the theory. Comparison of theoretical curves for neutral atoms and He-like ions shows that the influence of the outer-shell electrons is rather weak in this case, so it seems unlikely that the residual electron correlation can explain the discrepancy. The relativistic effects are large and change the form of the curve remarkably [15], but they are not large enough to bring theory into agreement with experiment.

More generally, our calculations show that the relative influence of the outer-shell electrons on $\mathcal{R}$, being significant for low-Z systems, gradually decreases as Z increases. This is what one might have anticipated, having in mind that the characteristic photon energy scales as Z^2, so that
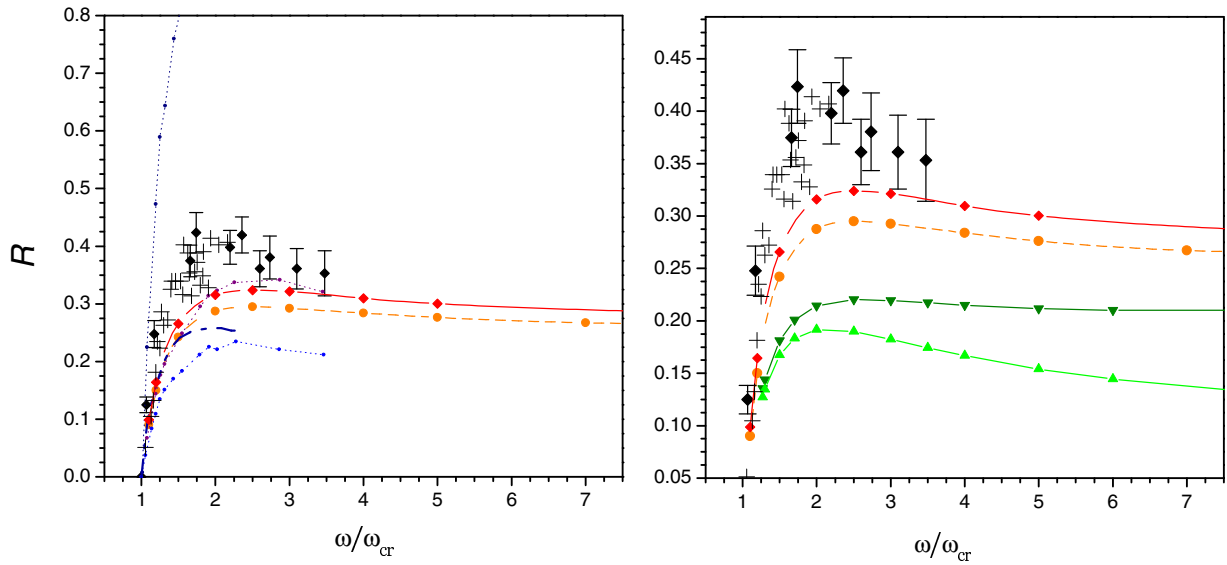
FIG. 3. (Color online) The same as Fig. 2 but for neutral calcium (Ca, $Z = 20$). The crosses denote the experimental results of Oura *et al.* [28]. On the left panel, the violet dash-dotted line denotes the calculation by Mikhailov *et al.* [22].

the interaction of electrons with the photon should become increasingly localized around the nucleus when Z increases.

It is interesting that for small and medium photon energies, $\omega/\omega_{cr} \lesssim 2$, the relativistic results for $\mathcal{R}$ exhibit essentially the same scaling law for neutral atoms as those reported previously for the nonrelativistic He-like ions [26,27]. In particular, the relativistic theoretical values of $\mathcal{R}$ for $\omega/\omega_{cr} = 2$ are nearly the same for all neutral atoms considered in the present work (about 0.35, see Table III). This is because, for low-Z atoms, the electron correlation effects are large and relativistic effects are small, whereas for medium-Z atoms, it is vice versa. Since both effects increase the ratio $\mathcal{R}$, the sum of them leads to a nearly uniform (in Z) enhancement of the familiar nonrelativistic He-like curve.

The situation becomes drastically different for large photon energies, $\omega/\omega_{cr} \gtrsim 2$. In this region, the $\mathcal{R}$ curve for light atoms decreases gradually, similarly to what is found for the well-studied nonrelativistic helium case. For heavy atoms, however, the relativistic effects change this behavior. Already for copper the familiar nonrelativistic peak of the curve around $\omega/\omega_{cr} = 2$ disappears (Fig. 4), while for silver the curve becomes monotonically increasing (Fig. 5). Our previous calculation [15] suggests that the relativistic curve increases monotonically also at higher energies, thus changing the asymptotic behavior with regard to the nonrelativistic theory.

We mention that in all experimental studies [11–13], the experimental data for $\mathcal{R}$ were fitted to semiempirical curves assuming the nonrelativistic behavior in the high-energy limit,
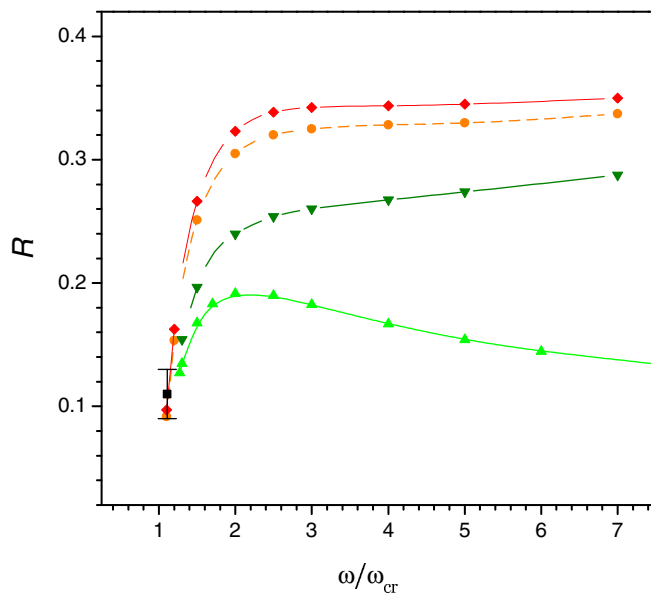

FIG. 4. (Color online) The same as Fig. 2 but for neutral copper (Cu, $Z = 29$). The experimental result is by Diamant *et al.* [29].
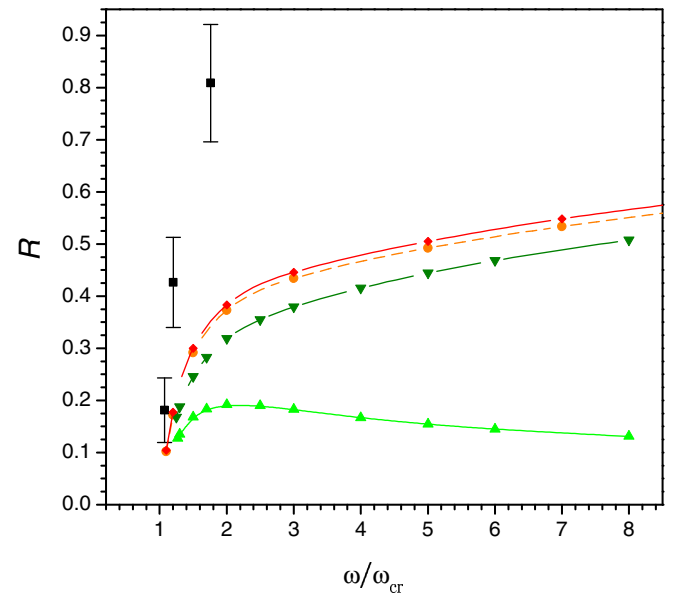

FIG. 5. (Color online) The same as in Fig. 4, but for neutral silver (Ag, $Z = 47$). The experimental points are by Kanter *et al.* [11].

which is not fully justified in the case of medium-Z atoms, according to our calculations.

V. CONCLUSION

We performed calculations of the double K-shell photoionization cross section for several neutral, medium-Z atoms from magnesium ($Z = 10$) up to silver ($Z = 47$). Our fully relativistic approach accounts for all multipoles of the absorbed photon as well as the retardation (the frequency dependence) of the electron-electron interaction. The electron-electron interaction was taken into account rigorously to the leading order of perturbation theory. The higher-order electron-electron interactions (in particular, with the outer-shell electrons) were treated approximately by means of some screening potential in the Dirac equation. The approach of this work is strictly gauge invariant, and this was utilized in order to cross-check the computational procedure.

The results of our computations are in reasonable agreement with experimental data [12,13,29] for the light elements, but they disagree strongly with the measurement of Ref. [11] for silver. The reason for this disagreement is unknown.

Our calculations predict large relativistic effects for copper ($Z = 29$) and for heavier atoms, as well as at large photon energies (more than twice larger than the double K-shell ionization energy). For these energies, the shape of the $\mathcal{R}$ curve is changed quite remarkably due to relativity. This prediction cannot be presently tested against experiment, as there have not been any direct measurements of double photoionization in this region so far.

[1] J. S. Briggs and V. Schmidt, J. Phys. B **33**, R1 (2000).

[2] J.-Z. Tang and I. Shimamura, Phys. Rev. A **52**, R3413 (1995).

[3] A. S. Kheifets and I. Bray, Phys. Rev. A **54**, R995 (1996).

[4] K. W. Meyer, C. H. Greene, and B. D. Esry, Phys. Rev. Lett. **78**, 4902 (1997).

[5] Y. Qiu, J.-Z. Tang, J. Burgdörfer, and J. Wang, Phys. Rev. A **57**, R1489 (1998).

[6] J. C. Levin, G. B. Armen, and I. A. Sellin, Phys. Rev. Lett. **76**, 1220 (1996).

[7] R. Dörner, T. Vogt, V. Mergel, H. Khemliche, S. Kravis, C. L. Cocke, J. Ullrich, M. Unverzagt, L. Spielberger, M. Damrau, O. Jagutzki, I. Ali, B. Weaver, K. Ullmann, C. C. Hsu, M. Jung, E. P. Kanter, B. Sonntag, M. H. Prior, E. Rotenberg, J. Denlinger, T. Warwick, S. T. Manson, and H. Schmidt-Böcking, Phys. Rev. Lett. **76**, 2654 (1996).

[8] J. C. Levin, I. A. Sellin, B. M. Johnson, D. W. Lindle, R. D. Miller, N. Berrah, Y. Azuma, H. G. Berry, and D.-H. Lee, Phys. Rev. A **47**, R16 (1993).

[9] J. A. R. Samson, W. C. Stolte, Z.-X. He, J. N. Cutler, Y. Lu, and R. J. Bartlett, Phys. Rev. A **57**, 1906 (1998).

[10] E. P. Kanter, R. W. Dunford, B. Krässig, and S. H. Southworth, Phys. Rev. Lett. **83**, 508 (1999).

[11] E. P. Kanter, I. Ahmad, R. W. Dunford, D. S. Gemmell, B. Krässig, S. H. Southworth, and L. Young, Phys. Rev. A **73**, 022708 (2006).

[12] J. Hoszowska, A. K. Kheifets, J.-C. Dousse, M. Berset, I. Bray, W. Cao, K. Fennane, Y. Kayser, M. Kavčič, J. Szlachetko, and M. Szlachetko, Phys. Rev. Lett. **102**, 073006 (2009).

[13] J. Hoszowska, J.-C. Dousse, W. Cao, K. Fennane, Y. Kayser, M. Szlachetko, J. Szlachetko, and M. Kavčič, Phys. Rev. A **82**, 063408 (2010).

[14] A. S. Kheifets, I. Bray, and J. Hoszowska, Phys. Rev. A **79**, 042504 (2009).

[15] V. A. Yerokhin and A. Surzhykov, Phys. Rev. A **84**, 032703 (2011).

[16] V. M. Shabaev, Phys. Rep. **356**, 119 (2002).

[17] J. Hata and I. P. Grant, J. Phys. B **17**, L107 (1984).

[18] F. Salvat, J. M. Fernández-Varea, and W. Williamson Jr., Comput. Phys. Commun. **90**, 151 (1995).

[19] V. A. Yerokhin, Phys. Rev. A **83**, 012507 (2011).

[20] V. A. Yerokhin and A. Surzhykov, Phys. Rev. A **82**, 062702 (2010).

[21] V. M. Shabaev, I. I. Tupitsyn, V. A. Yerokhin, G. Plunien, and G. Soff, Phys. Rev. Lett. **93**, 130405 (2004).

[22] A. I. Mikhailov, I. A. Mikhailov, A. N. Moskalev, A. V. Nefiodov, G. Plunien, and G. Soff, Phys. Rev. A **69**, 032703 (2004).

[23] M. Ya. Amusia, E. G. Drukarev, V. G. Gorshkov, and M. P. Kazachkov, J. Phys. B **8**, 1248 (1975).

[24] S. Fritzsche, Comp. Phys. Comm. **141**, 163 (2001); **183**, 1525 (2012).

[25] J. H. Scofield, Lawrence Livermore National Laboratory Report No. UCRL-51326, 1973 (unpublished); M. J. Berger, J. H. Hubbell, S. M. Seltzer, J. Chang, J. S. Coursey, R. Sukumar, D. S. Zucker, and K. Olsen, *XCOM: Photon Cross Sections Database* (National Institute of Standards and Technology, Gaithersburg), http://www.nist.gov/pml/data/xcom/.

[26] M. A. Kornberg and J. E. Miraglia, Phys. Rev. A **49**, 5120 (1994).

[27] A. I. Mikhailov, A. V. Nefiodov, and G. Plunien, J. Phys. B **42**, 231003 (2009).

[28] M. Oura, H. Yamaoka, K. Kawatsura, K. Takahiro, N. Takeshima, Y. Zou, R. Hutton, S. Ito, Y. Awaya, M. Terasawa, T. Sekioka, and T. Mukoyama, J. Phys. B **35**, 3847 (2002).

[29] R. Diamant, S. Huotari, K. Hämäläinen, C. C. Kao, and M. Deutsch, Phys. Rev. A **62**, 052519 (2000).